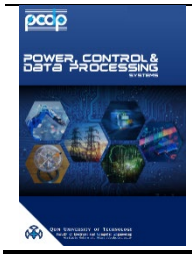
DOI: 10.30511/pcdp.2026.2085637.1065 - ISSN: 3060-8376 - Vol 3(4), 2026



POWER, CONTROL AND DATA PROCESSING SYSTEMS

Available Online at: https://pcdp.qut.ac.ir/

SOC and SOH Estimation of Lithium Battery: Innovative Hybrid Octave and LSTM Network

ARTICLE INFO

Article Type
Original Research

Authors
Amirhossein Rahimian Zarif [1*]
Seyed Mohammadreza Mousavi [2]
Javad Hamidzadeh

[1] Faculty of Electrical and Biomedical Engineering, Sadjad University, Mashhad, Iran, am.rahimian578@sadjad.ac.ir
[2] Faculty of computer engineering and information technology, Sadjad University, Mashhad, Iran, mo.mousavi271@sadjad.ac.ir
[3] Faculty of computer engineering and information technology, Sadjad University, Mashhad, Iran, j_hamidzadeh@sadjad.ac.ir

**** Correspondence***
Address: Faculty of Electrical and Biomedical Engineering, Sadjad University, Mashhad, Iran.
Phone: -
Fax: -
am.rahimian578@sadjad.ac.ir

Article History
Received: February 16, 2026
Accepted: June 16, 2026
ePublished: December 01, 2026

ABSTRACT

Accurately estimating the state of charge (SOC) and state of health (SOH) of lithium-ion batteries remains a significant challenge due to complex electrochemical dynamics and varying operational conditions. This research aims to overcome these challenges by proposing a novel hybrid neural network that combines octave convolution (OctConv) and long short-term memory (LSTM). The methodology begins with preprocessing battery voltage, current, temperature, internal impedance, and capacity data through outlier removal and min-max normalization, followed by partitioning into training, validation, and test sets. The OctConv module then decomposes the input into high- and low-frequency feature maps, enhancing extraction efficiency by reducing spatial redundancy. These multi-scale features are subsequently processed by LSTM layers to model both short-term fluctuations and long-term degradation trends across battery cycles. The model was trained using the Adam optimizer with MSE loss and ReLU activations and evaluated against established deep learning approaches, including OCT, LSTM, and CNN-LSTM, on the NASA dataset. Experimental results demonstrate the superior performance of the proposed OCT-LSTM model. It achieved significant improvements in SOC and SOH estimation, reducing the mean squared error (MSE) by 84.53% and 82.44%, respectively, compared to the CNN-LSTM benchmark. Furthermore, the model attained a 6.21% reduction in simulation parameters, highlighting greater parameter efficiency. The proposed method outperforms state-of-the-art approaches across multiple metrics, including the number of parameters, MSE, RMSE, MAE, prediction accuracy, and computational speed, demonstrating its potential as a significant advancement in this domain.

Keywords: State of Charge (SOC) Estimation, State of Health (SOH) Estimation, Lithium-Ion Battery (LIB), Convolutional Neural Networks (CNNs), Octave Convolution, Long Short-Term Memory (LSTM).

1 Introduction

Energy storage systems (ESSs) are pivotal technologies in advancing sustainable energy solutions, particularly for electric vehicles (EVs) and smart grids [1–6]. Among these, lithium-ion batteries (LIBs) have emerged as the most rapidly growing ESS technology, leveraged for their high energy density, long cycle life, and low self-discharge rates [7–9]. These attributes make LIBs indispensable for a wide range of applications, from portable electronics and industrial uses to hybrid and electric vehicles. The global transition toward renewable energy and the rising adoption of EVs have further solidified the importance of LIBs as a cornerstone of modern energy storage [10–13]. However, despite their advantages, critical challenges remain in battery safety and management for future demands. The state of charge (SOC) and state of health (SOH) are two fundamental parameters for ensuring safe and efficient operation of LIBs. SOC, representing the available capacity relative to nominal capacity, cannot be measured directly and must instead be estimated through advanced algorithms [14,15]. Accurate SOC estimation is essential for preventing hazardous conditions such as over-charging, over-discharging, and suboptimal battery performance [16]. Meanwhile, SOH serves as a key indicator of battery degradation and lifetime, directly influencing performance under varying operational conditions [17,18]. Precise SOH estimation is necessary to assess capacity fade and impedance increase, both of which impact system reliability. However, estimating these vital parameters remains challenging due to the nonlinear, time-variant behavior of LIBs and the interdependence between SOC and SOH [19–23].

Overcoming these challenges through robust estimation methods is critical for enhancing accuracy, prolonging battery lifespan, and ensuring safe operation across applications. SOC estimation methods are typically classified into three main categories: data-driven, adaptive, and hybrid approaches. Data-driven methods [24,25] can be further subdivided into direct measurement techniques such as Coulomb counting (CCM) [26,27], open-circuit voltage (OCV) [28–30], impedance methods [31,32], and model-based approaches [33,34]. Recent research has extensively explored SOC estimation, with prevailing methods falling into model-based, data-driven, and Coulomb-counting techniques. While model-based methods offer high accuracy by leveraging system-specific knowledge, their effectiveness is often limited by the challenges in developing precise system models. In contrast, data-driven methods reduce reliance on domain expertise by utilizing extensive process data, though they require large datasets for reliable performance. Coulomb-counting techniques, on the other hand, estimate battery capacity by integrating discharge current over time, providing a straightforward but sometimes less adaptive solution [35–38]. Capacity degradation during charge-discharge cycles is widely used for prediction, yet SOH remains challenging to estimate due to multiple influencing factors. Current approaches include model-based [39–42] and data-driven methods [43,44]. Model-based techniques, such as equivalent circuit [45,46] and electrochemical models [47–49], establish nonlinear relationships between measured signals and SOH by leveraging battery dynamics, including lithium-ion loss and material degradation. In contrast, data-driven methods rely on pattern recognition from large datasets [50–52].

1.1 Previous research

Extensive research has explored machine learning-based approaches for SOC and SOH co-estimation, with particular emphasis on modeling their complex nonlinear relationships. The continued focus on this problem reflects the fundamental challenges in developing machine learning (ML) methods that can effectively capture the coupled dynamics between these battery states. The study [53] aims to minimize dependence on initial conditions by first constructing two RBF-ARX models to represent battery dynamics and correlate SOC, SOH, and measured data. Target distributions are then derived, enabling initial state estimation via Markov chain Monte Carlo sampling. Finally, an unscented Kalman filter combined with an RBF-ARX model is proposed for SOC/SOH co-estimation. The paper [54] presents a co-estimation framework for SOC and SOH. A BiLSTM network, optimized via PSO, then estimates SOH and terminal voltage using cyclic and temporal data patterns. The optimized PSO-BiLSTM model subsequently serves as the basis for SOC estimation through an EKF algorithm. The research [55] presents a data-optimized SOC-SOH estimation method with current bias compensation. The impact of current bias on state estimation accuracy is analyzed, and the limitations of the Kalman filter are explained. An enhanced parameter identification framework is then developed, employing Fisher Information Matrix-based sensitivity analysis to select optimal data segments for iterative parameter refinement. In a relevant study [56] they developed a framework for rapid lithium-ion battery SOH estimation by formulating it as a multivariate Time Series Classification (TSC) problem. Their model, based on a Random Interval Classifier (RIC), was designed to operate exclusively on partial charging cycle data, specifically short sequences of voltage and temperature.

The study [57] employs a hybrid approach, coupling a fractional-order RC equivalent circuit model (ECM) of a LIB with a deep learning architecture. Model parameter identification is achieved through a modified particle swarm optimization algorithm, combining fractional-order dynamics and crisscross learning (FPSO-CL). The review paper [58] critically assesses multiple SOC estimation approaches, from established techniques such as Coulomb Counting and OCV measurement to sophisticated filter-based solutions and emerging data-driven methodologies. A detailed comparative analysis reveals the distinctive capabilities and inherent limitations of each approach. The work [59] proposes a distributed optimal Kalman consensus filter (KCF) for battery

management systems (BMS), along with a dynamic event-triggering mechanism (ETM) to reduce communication demands. The study [60] presents a joint SOC and SOH estimation approach for lithium-ion batteries, combining a temperature-dependent extended Kalman filter (EKF) with deep learning techniques. The paper [61] presents an EIS-based approach that integrates equivalent circuit modeling with data-driven methods for LIB SOH estimation. The work [62] presents an optimized BMS for high-power lithium battery energy storage (BES), utilizing a multi-head attention-augmented LSTM neural network alongside an adaptive unscented Kalman filter to achieve precise SOC and SOH estimation. The paper [63] optimized a Thevenin battery model to estimate OCV and SOH accurately. Methods like curve-fitting, ABC, PSO, DA, and GA were tested, with SOH defined by SOC, cycle count, capacity, and time. The paper [64] reviews contemporary advancements in SOC and SOH estimation techniques, analyzing cutting-edge approaches published within the recent years while critically examining their respective strengths and shortcomings.

The study [65] introduces an innovative SOC-OCV decoupling method for real-time SOC and SOH co-estimation in Li-ion batteries. A parallel neural network (PNN) framework is developed in [66] to predict the SOH and SOC in lithium-ion batteries concurrently. The approach employs a hybrid structure combining a back propagation neural network (BPNN) and an Elman neural network (ENN), while an adaptive Kalman filter (AKF) is applied to optimize SOC estimation. A residual-deep neural network (R-DNN)-based system is developed in [67] to assess the health status of lithium-ion batteries through analysis of temporal discharge patterns. Prior Studies [68–70] disregarded the importance of SOC and SOH monitoring for ESS operation. The current work resolves this oversight, demonstrating measurable gains in system performance metrics. A CNN-BiGRU neural network was implemented in article [71] to predict the SOH of LIBs. Temporal dependencies and data correlations were analyzed using voltage distribution and capacity variations extracted from discharge curves. In paper [72], parasitic side reactions at the charging negative electrode are examined as the primary focus. The performance of LSTM and recurrent neural network (RNN) architectures is compared, with LSTM being identified as more effective for extended sequence forecasting. A GWO-BP neural network-based SOH-SOC estimation model was developed in the article [73], where SOH estimation is integrated with the Ah method for capacity correction and improved accuracy. The study [74] employs a temperature-sensitive 2-RC model to characterize LIB degradation, enabling accurate SOH estimation across various chemistries. When extended to an N-RC framework and compared with 1-RC models, the 2-RC approach demonstrates superior accuracy and computational efficiency, as evidenced by numerical results.

A notable study [75] introduced a hybrid CNN-Attention-LSTM architecture. This method first selected highly correlated features via the Pearson correlation coefficient and normalized the data, establishing this method as a robust solution for SOH prediction. The previous study [76] has addressed the need for accurate battery SOH estimation in systems like PV and EVs. In this study, a hybrid parameter estimation technique was proposed for a semi-empirical Li-ion battery model. The model's parameters were optimized using the SCA algorithm, which resulted in superior performance compared to traditional models and other heuristic algorithms (GWO, DE, HHO, GA), achieving a higher SOH value. Previous research [77] has explored deep learning to overcome the limitations of conventional SOC estimation methods. A hybrid model integrating LSTM, GRU, and Attention mechanisms was developed. The model's robustness was confirmed via uncertainty analysis and subsequent feature optimization, establishing a highly accurate and efficient framework for SOC estimation. Previous work [78] tackled inaccurate SOC estimation in mining vehicle batteries, where high pulse discharging and over-discharge cause significant internal polarization. The authors proposed a hybrid closed-loop method, using an LSTM for offline modeling and a Sage-Husa AKF for online correction. To enable precise SOH estimation, the prior study [79] employed a stacking ensemble of LR, XGBoost, and RF, designed to capture the diverse linear, nonlinear, and long-temporal relationships in battery degradation. The model, which utilized a novel CPDE technique and grid search optimization, achieved significant performance improvements on real-time and NASA datasets.

1.2 Motivations and Contributions

Accurate and efficient estimation of the SOC and SOH is critical for the reliable operation of lithium-ion batteries. While data-driven methods have shown significant promise, a review of the literature reveals several persistent research gaps that limit their practical deployment. Specifically, existing approaches often face: (1) an architectural limitation in concurrently capturing multi-scale spatial features and long-term temporal dependencies; (2) an inherent trade-off between high estimation accuracy and high computational efficiency; and (3) a dependency on prior electrochemical knowledge or manufacturer-specific parameters, which restricts their general applicability. These identified gaps motivate the development of a novel hybrid framework in this study. To address these challenges, a novel hybrid neural network model that integrates Octave Convolution (OCT) with a Long Short-Term Memory (LSTM) network is proposed for accurate estimation of SOC. The same architecture is also shown to be effective for SOH estimation, based on our prior work [51].

The principal contributions of this paper are fourfold. First, a novel hybrid OCT-LSTM architecture is designed to effectively capture both short-term fluctuations and long-term degradation trends in battery data. This design overcomes the limitation of standard models in handling multi-scale spatiotemporal features. Second, a multi-channel, data-driven input structure is introduced, which utilizes key operational parameters—including voltage, current, temperature, internal

impedance, and capacity—to evaluate the battery's intrinsic characteristics. A key innovation of this approach is its operation without prior knowledge of the battery's internal electrochemical properties or manufacturer-provided specifications, thereby significantly reducing system complexity and enhancing general applicability across different battery types and conditions.

Third, the proposed methodology incorporates Octave Convolution (OCT) to decompose the input data into high- and low-frequency components. This innovation enhances feature extraction efficiency by reducing spatial redundancy, leading to a model that is both more accurate and more parameter-efficient. Finally, the performance of the proposed model has been comprehensively validated using the NASA battery dataset under real-world parameters. The experimental results demonstrate significant improvements in prediction accuracy, as measured by Mean Absolute Error (MAE), Mean Squared Error (MSE), and Root Mean Squared Error (RMSE), alongside gains in computational speed and parameter efficiency. This confirms the framework's effectiveness, precision, and practical viability for SOC estimation, with the architecture's effectiveness for SOH estimation reported as a separate validation.

This paper is organized in the following sequence: Section 2 introduces and evaluates the proposed Octave-LSTM-based approach. Section 3 details the battery dataset and thoroughly examines the SOC and SOH estimation methodology. Section 4 presents the experimental results, including learning techniques and comparative analyses. Section 5 analyzes the performance of the proposed network, compares SOC and SOH estimation accuracy, and evaluates the tested models. Ultimately, Section 6 concludes the study by summarizing the key findings and outlining future work.

2 Suggested Approach

The SOC represents the remaining energy stored in a battery. Physically, it is quantified as the ratio of the average lithium-ion concentration in the cathode to the maximum possible concentration. Thus, the SOC can also be interpreted as the proportion of residual energy relative to the battery's total usable capacity. The SOH estimation, however, relies on data-driven models that utilize comprehensive battery datasets to predict Remaining Useful Life (RUL) [80,81]. This section details the OCT-LSTM-based SOC and SOH estimation framework, which encompasses data preprocessing, model training, SOC estimation, and battery health assessment [82–84]. The preprocessing stage involves outlier removal and data normalization, followed by partitioning the dataset into training, validation, and testing subsets. Input features include voltage, current, temperature, capacity, and internal impedance. Model performance is assessed by comparing predictions across different phases. The proposed approach employs Octave Convolution (OctConv) in place of traditional convolution, which reduces computational complexity while achieving superior performance compared to existing state-of-the-art methods.

2.1 Octave Convolution Network

OctConv network offers a more efficient alternative to traditional convolution layers by significantly reducing spatial complexity and computational overhead in Convolutional Neural Networks (CNNs) [85,86]. By decomposing feature maps into high frequency and low frequency components, OctConv enhances feature extraction efficiency while expanding the receptive field, leading to improved performance across diverse applications, including time-series analysis, medical imaging, remote sensing, image compression, and spectral image classification [87,88]. The proposed architecture advantages OctConv to process multi-frequency features efficiently, followed by Long Short-Term Memory (LSTM) layers to model temporal dependencies. This hybrid approach optimizes data processing efficiency by capturing both fine-grained details and long-range patterns, making it particularly suitable for sequential and high-dimensional data analysis. The input tensor X has dimensions (B, T, F, C), where B denotes the batch size, T represents the time dimension, F corresponds to the feature dimension, and C indicates the channel dimension (where C=1 in this case), as formalized in equation (1).

$$X \in R^{B\times T\times F\times C} \tag{1}$$

The initial layer employs an OctConv operation that spectrally decomposes the input tensor X into high frequency (X_H) and low frequency (X_L) components. This decomposition is mathematically formulated in equations (2) and (3).

$$\begin{aligned} &X_H = X \\ &Shape:(B,T,F,1) \end{aligned} \tag{2}$$

$$\begin{aligned} &X_L = \downarrow 2(x) \\ &shape(B,\frac{T}{2},\frac{F}{2},1) \end{aligned} \tag{3}$$

The OctConv layer is configured with a kernel size of (4, 1), 40 convolutional filters, an octave ratio parameter = 1, and an output low-frequency ratio of 0.5. This frequency-based decomposition enables more efficient feature extraction by processing high- and low-frequency components separately while maintaining their spatial relationships. In this decomposition, X_H preserves the high-frequency spatial details while X_L contains the low-frequency components generated through down sampling of the input tensor X. The dimensional characteristics of these components are defined as X_H: (B, T, F, 1) and X_L: (B, T/2, F/2, 1). The architecture implements parallel convolutional pathways to process these frequency components independently. Four distinct convolution operations are employed: High-to-high (H→H), High-to-low (H→L), Low-to-high (L→H), Low-to-low (L→L). The high-to-high convolution operation, which processes fine-grained spatial features within the high-frequency domain, is mathematically represented in equation (4).

$$Y_H^{HH} = W_{HH} * X_H \quad Shape(B,T,F,filters) \tag{4}$$

This multi-branch approach enables comprehensive feature extraction across different frequency bands while maintaining computational efficiency. Here, W_{HH} represents the convolutional weight matrix for the high-to-high frequency pathway, where $*$ indicates the convolution operator. The output Y_H^{HH} has dimensions (B, T, F, filters). Similarly, the high-to-low frequency convolution is defined as equation (5):

$$Y_L^{HL} = \downarrow 2(W_{HL} * X_H) \quad shape(B,\frac{T}{2},\frac{F}{2},filters) \tag{5}$$

Here, W_{HL} denotes the convolutional weight matrix for the high-to-low frequency pathway. The resulting output Y_L^{HL} has dimensions (B, T/2, F/2, filters), where the down-sampling operation is indicated by the downward arrow ($\downarrow$). The low-to-high frequency convolution is defined as equation (6):

$$Y_H^{LH} = \uparrow 2(W_{LH} * X_L) \quad shape(B,T,F,filters) \tag{6}$$

Parameter W_{LH} represents the convolutional weight matrix for the low-to-high frequency pathway, producing output Y_H^{LH} with dimensions (B, T, F, filters). The up-sampling operation is indicated by an upward arrow ($\uparrow$). Similarly, the low-to-low frequency convolution is defined as equation (7):

$$Y_L^{LL} = W_{LL} * X_L \quad shape(B,\frac{T}{2},\frac{F}{2},filters) \tag{7}$$

The low-to-low frequency pathway is characterized by the convolutional weight matrix W_{LL}, which generates output Y_L^{LL} with dimensions (B, T/2, F/2, filters). The convolution outputs are then integrated to construct both high-frequency and low-frequency feature maps through the following combination process. The high-frequency feature map is computed as in equation (8):

$$Y_H = Y_H^{HH} + Y_H^{LH} \quad shape(B,T,F,filters) \tag{8}$$

The high-frequency output Y_H maintains dimensions (B, T, F, filters), while the low-frequency feature map is formulated as equation (9):

$$Y_L = Y_L^{HL} + Y_L^{LL} \quad shape(B,\frac{T}{2},\frac{F}{2},filters) \tag{9}$$

The low-frequency output Y_L preserves its original dimensionality (B, T/2, F/2, filters). The composite feature map Y is generated through the integration of both high-frequency and low-frequency components, as expressed in equation (10):

$$Y = Y_H + \uparrow 2(Y_L) \quad shape(B,T,F,filters) \tag{10}$$

The up-sampling operation aligns the spatial dimensions of Y_L with those of Y_H, producing a unified feature map Y with the shape (B, T, F, filters). Through the combined operations defined in (9) and (10), the framework incorporates low-frequency components into the high-frequency domain via successive up-sampling and convolutional transformations. The proposed framework employs octave convolution to decompose input signals into high- and low-frequency components, significantly reducing computational overhead. This decomposition is particularly advantageous for battery data analysis, where low-frequency components typically dominate. The method proves valuable for simultaneous SOH and SOC monitoring by enabling scalable and efficient processing. The octave convolution architecture enhances multi-scale feature extraction through independent frequency processing, which simultaneously improves detection of both transient abnormalities and gradual degradation patterns. Furthermore, it reduces feature map redundancy by generating compact yet highly discriminative representations, leading to better model generalization and improved prediction accuracy. Comparative evaluations demonstrate that this approach outperforms conventional methods in both estimation accuracy and efficiency for SOC and SOH prediction tasks.

2.2 Implementation Criteria

The proposed method comprises three key stages: preprocessing, training, and estimation, as illustrated in Fig. 1.

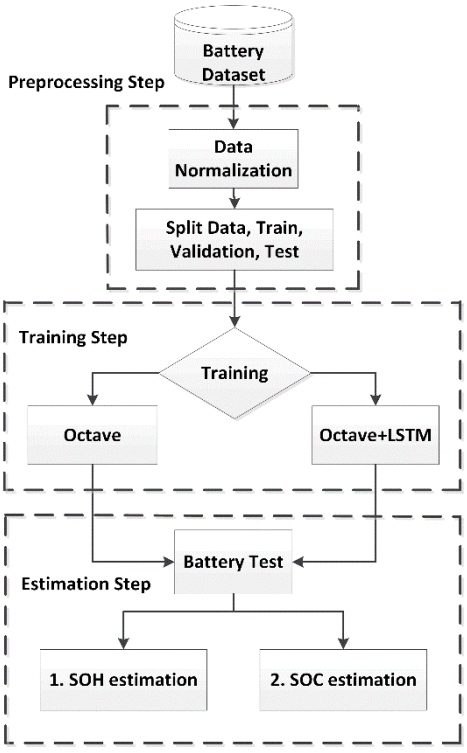


Fig. 1 Block diagram of the OCT-LSTM proposed Network, where the NASA battery dataset is fed into the system. The diagram consists of three main stages: preprocessing, training, and SOH/SOC estimation of the battery

In the preprocessing phase, battery-related parameters, including voltage, current, temperature, internal Impedance, and capacity, are normalized using equation (11). In (11), the

set X_i^k is defined, where n denotes the number of samples per cycle, and x represents the collection of all charge cycles.

$$z_i^k = \frac{X_i^k - \min(x)}{\max(x) - \min(x)} \rightarrow i \in \{1, ..., n\} \quad (11)$$

Following parameter estimation, the data undergoes a de-normalization procedure. Subsequently, the dataset is partitioned into three subsets: training, validation, and test sets. Batteries 5, 6, and 7 were employed for training, while Battery 18 was reserved for evaluating the SOH and SOC parameters. Prior to network input, the data was normalized to ensure optimal processing. During the training phase, key battery features, including charge voltage, discharge voltage, current, and temperature, were extracted from the dataset and fed into the network as input variables. The proposed architecture combines Octave Convolution and LSTM layers, forming an integrated Octave+LSTM network. This hybrid approach significantly reduces the number of trainable parameters while improving computational efficiency, thereby accelerating training speed without compromising accuracy. The model's performance was evaluated by estimating SOH and SOC, and the results were benchmarked against existing methods in the field. A comprehensive analysis of the outcomes is presented to validate the efficacy of the proposed framework.

3 NASA Battery Dataset

The present study investigates critical battery performance metrics, including voltage, charge-discharge current, capacity fade, internal impedance, and thermal behavior for accurate SOC and SOH assessment.

3.1 Initial and Working Conditions

The analysis utilizes the publicly available NASA Li-ion battery dataset, originally compiled by the Prognostics Center of Excellence (PCoE). The experimental data were obtained from 18650 Li-Cobalt cells, LG Chem, with 2100mAh nominal capacity, and 4.20V cutoff voltage, manufactured by the Idaho National Laboratory [89]. Comprehensive battery specifications are provided in Table 1, with additional experimental details documented in [90]. For model validation purposes, four representative cell samples, designated B0005, B0006, B0007, and B0018, were subjected to systematic testing protocols.

The charging protocol involved constant current (CC) charging at 1500 mA until the upper cut-off voltage of 4.20 V was reached, followed by constant voltage (CV) charging at 4.20 V until the current tapered to 20 mA. In contrast, the discharge protocol was a constant current (CC) discharge at 2000 mA with specific discharge cut-off voltages of 2.70 V for B0005, 2.50 V for B0006, 2.20 V for B0007, and 2.50 V for B0018. Comprehensive test parameters are documented in Table 2. In accordance with the dataset specifications, battery end-of-life (EOL) was defined as the point at which the available capacity degraded to 70% of the nominal 2000mAh rating. For dataset usage, batteries B0005, B0006, and B0007 were used for training, while B0018 was reserved for testing and validation.

Table 1 NASA battery dataset characteristics, including individual cell specifications and test parameters [90]

Battery number	Condition			
	Maximum voltage (V)	*Minimum voltage (V)*	*Discharge current (mA)*	*Capacity (mAh)*
B0005	4.20	2.70	2000	2000
B0006	4.20	2.50	2000	2000
B0007	4.20	2.20	2000	2000
B0018	4.20	2.50	2000	2000

Table 2 Specifications of the batteries tested for the NASA dataset collection

Battery Properties	18650 LIB
Production	LG Chem
Chemistry	18650 Li-Cobalt oxide
Nominal capacity	2100 mAh
Working voltage	3.00 - 4.20 V

The battery's SOC is quantified using a percentage-based metric, with 100% representing maximum charge capacity following a complete charging cycle and 0% indicating full discharge. Throughout both charging and discharging operations, key operational parameters, including battery voltage, current, impedance, and temperature, undergo continuous temporal variations. These measurable variables serve as critical inputs for state-of-charge determination. The fundamental relationship governing SOC calculation is formally expressed in equation (12). Hence, parameter Q_r signifies the remaining battery charge or remaining charge capacity, and parameter $Q_{nominal}$ corresponds to the nominal capacity of the battery.

$$SOC(\%) = \frac{Q_r}{Q_{nominal}} \times 100 \quad (12)$$

The estimation of SOH involves evaluating degradation metrics such as capacity loss and increased internal impedance, which serve as key indicators of battery performance degradation. As shown in Fig. 2, the progressive deterioration of battery capacity during discharge cycles, which is mathematically expressed by (13) as SOH, plays a critical role in accelerating the reduction of the remaining useful life (RUL) of the battery [91]. In Equation (13), parameter C_r denotes the battery's rated capacity, while C_c corresponds to the empirically derived capacity for each discharge cycle.

$$SOH(\%) = \frac{C_r}{C_c} \times 100 \quad (13)$$

As displayed in Fig. 2, the measured capacities of batteries B0005, B0006, B0007, and B0018 exhibit non-linear degradation patterns, indicating that capacity fade does not follow a consistent trajectory across cycles.

Moreover, the estimation of SOH is complicated by regenerative phenomena, undermining the dependability of conventional cycle-based assessment techniques. Even

marginal enhancements in estimation accuracy can substantially improve capacity prediction. Consequently, given the inherent complexities introduced by parasitic side reactions, data-driven approaches offer superior reliability by explicitly modeling these nonlinear effects. During the initial discharge cycle, battery B0005 demonstrated a starting capacity of 1.8565 Ah, which declined to 1.2875 Ah following charge-discharge cycling. A comparable reduction was observed in B0006, with its capacity diminishing from 2.0353 Ah to 1.1538 Ah. For B0007, recorded measurements showed an initial capacity of 1.8911 Ah, decreasing to 1.4005 Ah after testing. Lastly, B0018 exhibited the initial capacity of 1.8550 Ah, which subsequently reduced to 1.3411 Ah.

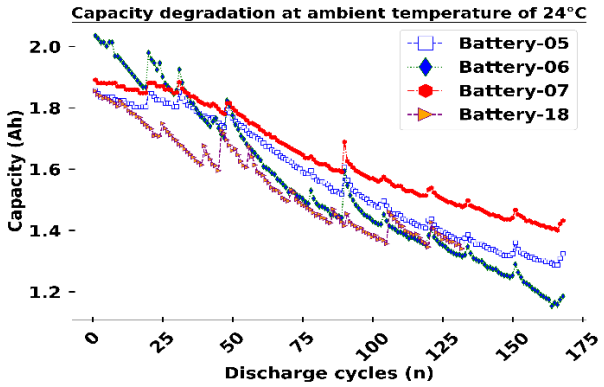


Fig. 2 Capacity measurement results for all battery cells in the NASA dataset

4 Experimental Results

To assess model performance across different deep learning frameworks, several neural network architectures were tested, including OCT, LSTM networks, and hybrid variants including CNN-LSTM and OCT-LSTM. The experiments were conducted on Google Colab's cloud-based platform, which provided a Linux environment with 128GB of system memory and an NVIDIA Tesla P100 GPU with 16GB of memory for accelerated computation.

4.1 Key Parameters

The Adam optimizer was adopted due to its proven efficiency and robustness in training complex hybrid architectures that combine convolutional and recurrent layers for time-series forecasting, a characteristic common in battery SOC and SOH estimation tasks. A fixed learning rate of 0.001 was empirically determined to be optimal, minimizing the MSE loss function. Preliminary experiments confirmed that higher learning rates led to unstable convergence, while lower values resulted in excessively slow training and poorer generalization performance on the validation set. The OctConv layer was configured with a kernel size of (4, 1) and 40 convolutional filters. The octave ratio was set to 1, and the output low-frequency ratio to 0.5. This configuration was found to optimally balance the processing of high- and low-frequency features, a design choice that aligns with efficiently modeling the multi-scale characteristics of battery data. The batch size was set to 50, representing a compromise between gradient stability and computational efficiency, since very small batches produced noisy gradients and very large batches increased memory demands without improving performance.
The model was trained for 500 steps, as this was the point at which the validation loss consistently plateaued in our preliminary analyses. This early stopping criterion ensures that the model achieves sufficient convergence while rigorously avoiding overfitting. ReLU activation functions were employed to mitigate vanishing gradient issues and ensure efficient computation, in line with common practice in deep learning-based estimation frameworks. Concurrently, these parameter choices reflect a balance between theoretical justification and experimental validation, thereby ensuring the reproducibility and reliability of the proposed model.
For quantitative evaluation, three key error metrics were utilized: MSE, RMSE, and MAE. Specifically, Equation (14) provides the mathematical formulation for MSE, while Equation (15) presents RMSE. Both metrics serve to quantify the prediction accuracy by measuring the deviation between modeled capacity estimates of the battery in Ah (y_i) and the actual capacity ($\hat{y}_i$). Within these mathematical formulations, the parameter (n) denotes the total number of charge-discharge cycles experimentally recorded for individual battery cells. Equation (16) introduces the MAE as an alternative robustness measure for comparative analysis.

$$MSE = \frac{1}{n}\sum_{1}^{n}\left(y_i - \hat{y}_i\right)^2 \tag{14}$$

$$RMSE = \left(\frac{1}{n}\times\sum_{1}^{n}(y_i - \hat{y}_i)^2\right)^{\frac{1}{2}} \rightarrow i \in \{1,2,...,n\} \tag{15}$$

$$MAE = \frac{1}{n}\sum_{1}^{n}\left|y_i - \hat{y}_i\right| \tag{16}$$

4.2 SOC Estimation

This section provides a rigorous comparative evaluation of diverse neural network architectures for battery SOC estimation, assessing their predictive accuracy, computational efficiency, and performance. The proposed SOC estimation methodology was implemented and evaluated through systematic testing protocols. For model development, three lithium-ion batteries (B0005, B0006, and B0007) were utilized in the training phase. Validation was subsequently performed using Battery B0018 as an independent test case to objectively assess estimation accuracy. A multi-metric validation approach was implemented, utilizing complementary error measures including MSE, RMSE, and MAE, ensuring robust performance characterization. The experimental protocol incorporated four distinct charge-discharge cycles, including cycles 1, 50, 100, and 130, representing different stages of battery operation. This multi-cycle evaluation framework enables a comprehensive assessment of the SOC estimation

algorithm's robustness across varying operational conditions. The complete set of estimation results is presented in Figs. 3 to 6, providing detailed graphical representations.

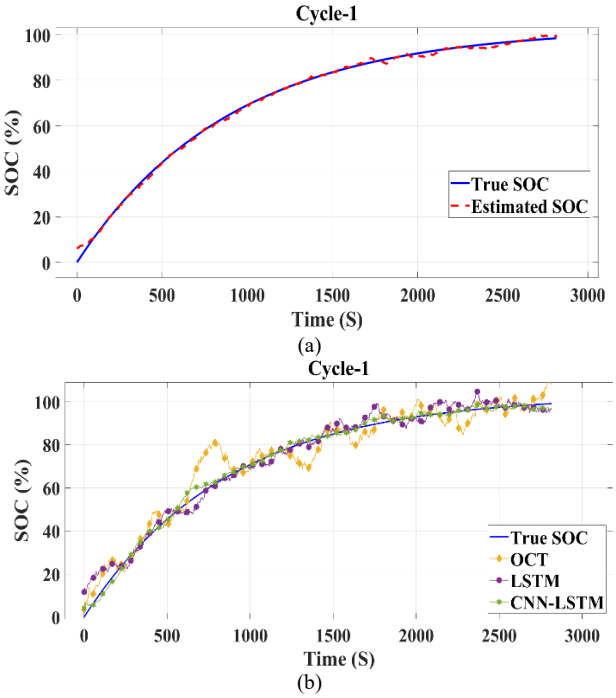


Fig. 3 Illustration of the battery SOC estimation in percentage, (a) compares the estimated SOC of the proposed method with the actual SOC during the initial charge cycle, (b) estimated SOC of the OCT, LSTM, and CNN-LSTM networks with the actual SOC

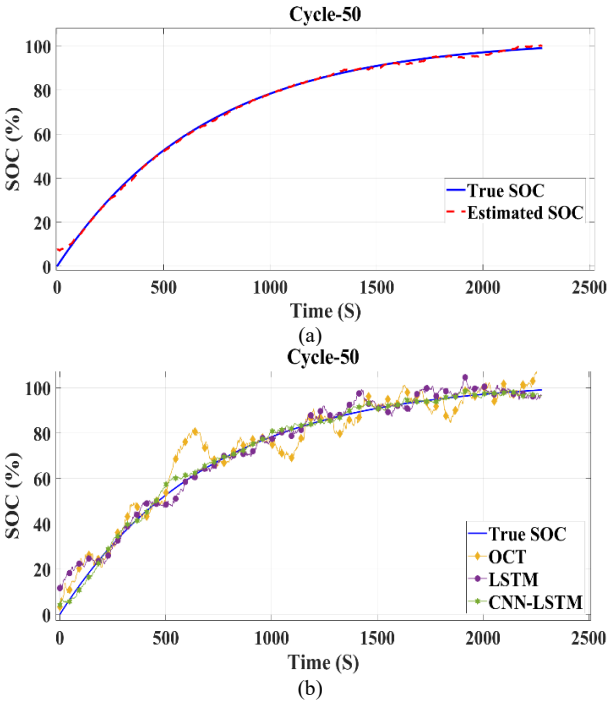


Fig. 4 Assessment of SOC estimation robustness: Comparison of predicted SOC versus actual SOC for the 50th charge cycle. (a) proposed method in comparison with the actual SOC, and (b) OCT, LSTM, and CNN-LSTM networks with the actual SOC

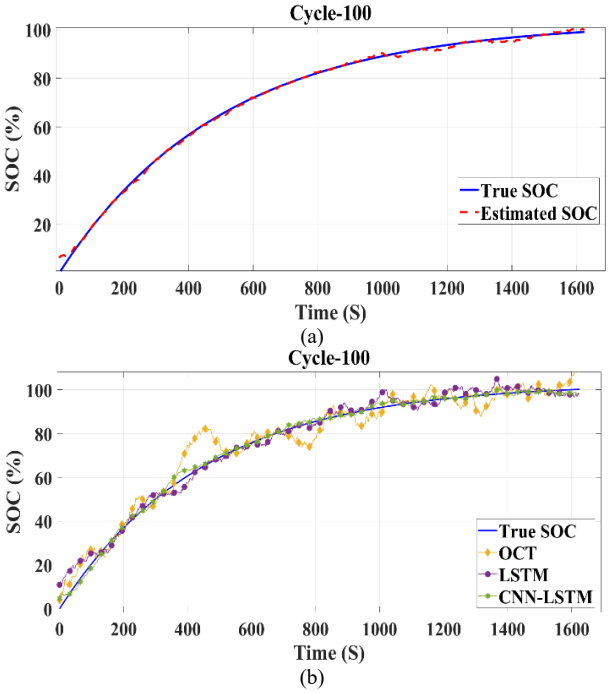


Fig. 5 Comparison of estimated SOC versus actual SOC for the 100th charge cycle. (a) proposed method compared to the actual SOC, and (b) OCT, LSTM, and CNN-LSTM networks compared to the actual SOC

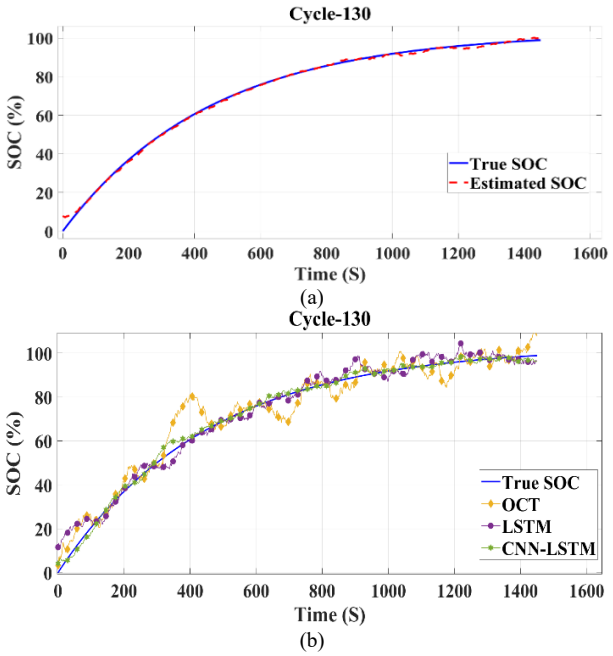


Fig. 6 The SOC estimation accuracy at the 130th cycle, showing the comparison of actual SOC with (a) the proposed method and (b) OCT, LSTM, and CNN-LSTM networks

Fig. 3(a) compares the SOC prediction with the actual SOC during the initial charging cycle, performed by the proposed method using the battery dataset. The x-axis denotes the charging duration in seconds, while the y-axis displays the SOC in percentage, scaled from 0% to 100%. The results indicate remarkably precise SOC estimation. On the other

hand, Fig. 3(b) displays the SOC estimation for the first cycle using OCT, LSTM, and CNN-LSTM networks. As shown in the figure, although the OCT network reduces computational error, it still does not deliver an accurate SOC value. In contrast, the LSTM and CNN-LSTM networks achieve much better results, with a significant decrease in computational error. The hybrid CNN-LSTM network, as depicted in this figure, exhibits high precision in SOC estimation with the lowest fluctuations. Subsequent Figs. 4, 5, and 6 depict the SOC estimations for the 50th, 100th, and 130th charge cycles, respectively. Accordingly, Figs. 4(a), 5(a), and 6(a) show a comparison between the estimated SOC using the proposed network and the actual SOC values. Besides, Figs. 4(b), 5(b), and 6(b) display the SOC estimation results from the OCT, LSTM, and CNN-LSTM networks compared to the battery's actual capacity. The findings consistently highlight the proposed method's effectiveness, achieving both high accuracy and computational efficiency in SOC prediction across multiple cycles.

The performance of various neural networks in estimating the SOC of lithium-ion batteries is presented in Table 3. This table indicates the MSE error values computed for the evaluated neural networks. The results indicate that the OCT network shows an error rate of 5.21% while both LSTM and CNN-LSTM networks demonstrate significantly lower errors of 0.0594% and 0.0362%, respectively. Most notably, the proposed network achieves an exceptional precision level with a minimal error of 0.0056%, representing a remarkable improvement in the SOC estimation accuracy for lithium-ion batteries. The RMSE error rate shown in Table 3 highlights the exceptional performance of the proposed method over the other OCT, LSTM, and CNN-LSTM networks. The evaluation results indicate that the proposed methodology achieves a substantially lower error of merely 0.749%. Table 3 also displays the comparative MAE analysis across the evaluated networks. The proposed method demonstrates superior performance with a minimal error of 0.60%. In addition, the remaining networks, OCT, LSTM, and CNN-LSTM, exhibit error rates of 18.509%, 1.927%, and 1.331%, respectively.

Table 3 Evaluation results of different tested networks for battery SOC estimation

Algorithm	PARAMETERS			
	MSE (%)	*RMSE (%)*	*MAE (%)*	*Number of parameters*
OCT	5.21	22.301	18.509	356364
LSTM	0.0594	2.438	1.927	36036
CNN-LSTM	0.0362	1.902	1.331	41228
OCT-LSTM	0.0056	0.749	0.6	38668

Table 3 also reveals that the proposed network exhibits a remarkable reduction in the number of parameters, containing only 38,668 parameters. This substantial reduction in parameter count, combined with the observed improvement in estimation accuracy, underscores the proposed network's enhanced computational efficiency and precision in SOC estimation relative to conventional approaches.

4.3 SOH Estimation

The present section systematically reports the performance outcomes of various neural network configurations implemented for battery SOH assessment. Quantitative evaluation was conducted using three established error metrics: MSE, RMSE, and MAE. For better comparison, the architecture of each network is characterized with full disclosure of its number of parameters. The comparative analyses presented in Figs. 7 and 8 demonstrate the capacity estimation capabilities of four distinct deep learning architectures: OCT, LSTM, CNN-LSTM, and OCT-LSTM. Fig. 7 thoroughly highlights significant variations in predictive accuracy across network architectures, particularly evident during battery regeneration phenomena. Furthermore, the figure provides critical insights into both the comparative evaluation and validation of network performance metrics. To validate the performance of the proposed framework, Fig. 8 especially compares the estimated battery health levels with actual capacity measurement. The presented neural architecture exhibits superior SOH estimation precision, outperforming all tested networks.

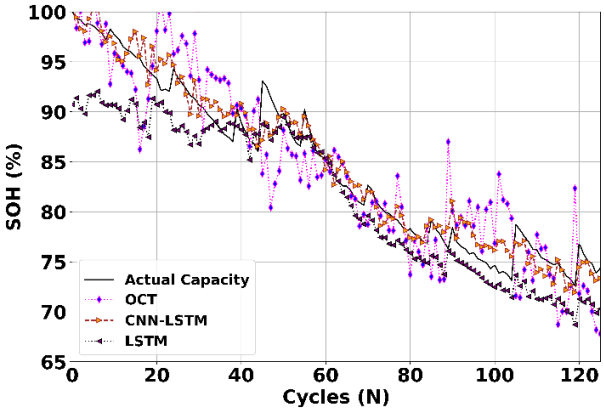


Fig. 7 The SOH estimation of battery B0018 compared to its actual capacity, as assessed by OCT, LSTM, and CNN-LSTM neural networks

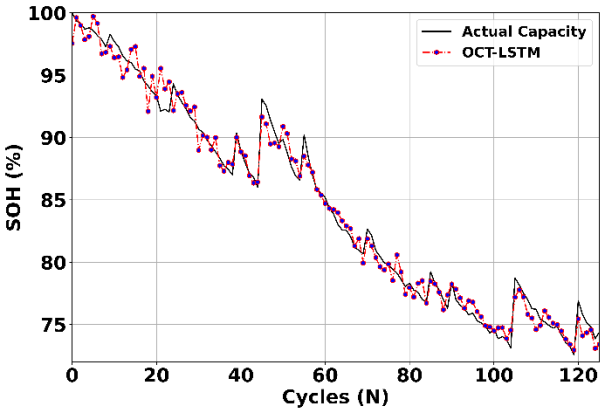


Fig. 8 Comparison analysis between the estimated SOH of battery B0018 derived from the proposed model and its actual capacity

Among these configurations, the OCT-LSTM architecture achieves superior estimation accuracy, while the OCT model exhibits significantly greater variance in its predictive performance. Notably, the standalone LSTM implementation outperforms the OCT architecture, a finding attributable to LSTM's inherent ability to capture temporal dependencies in sequential data—a critical advantage for time-series regression tasks. The hybrid architecture demonstrates that combining OCT feature extraction with LSTM's temporal processing capabilities yields optimal performance, with OCT-LSTM emerging as the most effective configuration.

Table 4 compares the MSE across evaluated networks. The OCT network shows a 4.74% error, while the LSTM and CNN-LSTM networks achieved 0.614% and 0.4319% MSE, respectively, exhibiting progressively better performance. The proposed network establishes state-of-the-art performance with a remarkable 0.0758% MSE. Table 4 also presents the comparative RMSE analysis across evaluated network architectures. The OCT network shows an error rate of 21.772% while subsequent architectures demonstrate progressive improvements: the LSTM network with 7.837% and the CNN-LSTM network with 6.57%. The proposed architecture achieves optimal performance with 2.75% RMSE, representing a significant reduction in estimation error. The error comparisons in Table 4 show significant variation in MAE among different networks. Analyses reveal that the proposed architecture achieves the lowest recorded MAE with 1.946%. This performance hierarchy suggests that architectural differences significantly influence estimation accuracy, with OCT-based models showing particular achievement for this application. Notably, the hybrid architectures CNN-LSTM and OCT-LSTM demonstrate greater model complexity relative to the standalone LSTM, which correlates with their enhanced predictive capability.

Table 4 Comprehensive statistical analysis of experimental findings in lithium battery SOH assessment

Algorithm	PARAMETERS			
	MSE (%)	*RMSE (%)*	*MAE (%)*	*Number of parameters*
OCT	4.74	21.772	17.872	356364
LSTM	0.614	7.837	6.085	36036
CNN-LSTM	0.4319	6.57	5.547	41228
OCT-LSTM	0.0758	2.75	1.946	38668

Fig. 9 provides a comparative analysis of the simulation parameter counts across the evaluated network architectures. The data reveals that the OCT, LSTM, and CNN-LSTM networks contain 356364, 36036, and 41228 parameters, respectively. Most notably, the proposed OCT-LSTM network achieves a significant parameter reduction, employing only 38668 parameters. This represents a 6.21% decrease relative to the CNN-LSTM hybrid network, demonstrating enhanced parameter efficiency while maintaining network performance. Most significantly, the OCT-LSTM architecture achieves superior performance with the minimum error rate and the lowest number of parameters, establishing it as the most effective configuration for this application. This performance hierarchy highlights the critical influence of architectural design on estimation accuracy.

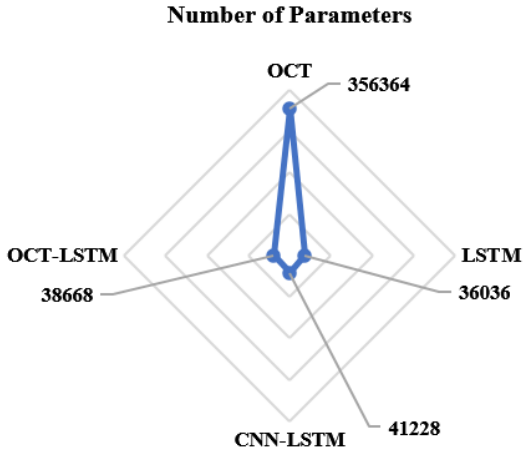


Fig. 9 Examining the differences in the number of simulation parameters among the tested OCT, LSTM, CNN-LSTM, and OCT-LSTM networks

Table 5 presents a detailed comparison between the proposed framework and contemporary approaches in battery estimation. X. Zhang et al. [73] used a hybrid dataset comprising 1,278 self-collected experimental samples from six 18650 batteries, along with public datasets from NASA and CALCE. The GWO-BP network was trained on the self-collected data and tested on NASA battery B0005 and CALCE data. Their experimental results showed that the proposed estimation model achieved an SOH estimation RMSE of 3.44%. Z. Bao et al. [71] proposed a model that was evaluated on two public datasets, namely the NASA Battery Dataset and the Oxford Battery Dataset. They trained the model on nine batteries (B0005, B0006, B0018, B0025, B0027, B0029, B0030, B0031, B0034) and tested it on four batteries (B0007, B0028, B0032, B0036), achieving an overall RMSE of 3.21%. The paper by L. Zhang et al. [72] trained and tested its model on the NASA dataset (B5 and B6 cells) and the CALCE dataset. For the NASA dataset, the reported RMSE values were 3.423% for B5 and 4.113% for B6.

S. Amir et al. [74] proposed a model that was trained on the initial cycle of Vendor 4 pouch cells from the CALCE dataset and B0005–B0018 from the NASA dataset, and then tested on the remaining cycles of the same Vendor 4 cells, as well as on Vendor 2 cells. The minimum achieved RMSE for SOH estimation was 3.85%. The method proposed by A. Petrella et al. [56] was trained on the NASA dataset (four cells: B0005, B0006, B0007, and B0018). The model was trained on three cells and tested on the remaining one, yielding a mean RMSE of 6.66%, with individual cell RMSE values of 2.82% (B0005), 6.44% (B0006), 3.30% (B0007), and 14.10% (B0018). As can be seen, the introduced network model demonstrates the highest accuracy, with a significantly reduced RMSE relative to existing approaches.

Initial benchmarking of the OCT architecture revealed its prediction accuracy on the tested dataset. Following this evaluation, established operational data were employed across three neural network configurations: LSTM, CNN-LSTM, and OCT-LSTM. Performance analysis demonstrated that the OCT-LSTM hybrid architecture achieved the lowest error margin among the evaluated models. Notably, this architecture maintained this performance advantage while utilizing fewer simulation parameters than the other networks. While the conventional LSTM implementation showed the most parameter-efficient design, it underperformed relative to both hybrid configurations in terms of prediction accuracy. Under the tested conditions, the OCT-LSTM architecture delivered competitive estimation precision coupled with computational efficiency, demonstrating its potential as an effective solution for battery health (SOH) and SOC prediction.

Table 5 Performance outcomes of the proposed method compared to previous research

Research	Procedure	RMSE (%)
X. Zhang et al., [73]	GWO-BP	3.44
Z. Bao et al., [71]	CNN-BiGRU	3.21
L. Zhang et al., [72]	LSTM	3.423 and 4.113
S. Amir et al., [74]	Two-RC	3.85
A. Petrella et al., [56]	TSC	6.66
Proposed Method	**OCT-LSTM**	**2.75**

5 Discussion

The comparative analysis reveals distinct performance disparities among the four evaluated architectures: OCT, LSTM, CNN-LSTM, and OCT-LSTM. Especially, the CNN-LSTM model outperforms the standalone LSTM, reducing MSE by 39.06% for SOC estimation and 29.66% for SOH estimation, and the RMSE by 23.40% for SOC estimation and 16.17% for SOH estimation. The results from the OCT-LSTM network show a notable improvement over CNN-LSTM on the tested dataset, with 82.44% reduction in MSE for SOH estimation, and 84.53% reduction for SOC estimation, and 58.14% decrease in RMSE for SOH estimation, and 60.62% decline for SOC estimation. Additionally, the OCT-LSTM achieves greater parameter efficiency compared to the CNN-LSTM by 6.21% reduction in the number of parameters, further highlighting its speed in computational optimization. When benchmarked against the conventional LSTM, the OCT-LSTM provides 90.57% lower MSE rate for SOC estimation and 87.65% for SOH estimation, and 69.28% reduction in RMSE for SOC estimation and 64.91% for SOH estimation, indicating that the OCT-LSTM is a highly effective model among those tested for this application.

The comparative evaluation shows that the proposed methodology achieves competitive RMSE values relative to contemporary approaches under the conditions tested. Within the scope of this study, the OCT-LSTM framework outperforms the traditional LSTM architectures tested. Specifically, the OCT-LSTM approach demonstrates advantages in error minimization, computational efficiency, and prediction accuracy compared to the baselines evaluated in this work. These findings highlight the potential of the proposed OCT-LSTM network for precise SOC and SOH estimation in lithium-ion batteries, pending further validation under additional operating conditions and battery types.

Despite the promising results demonstrated by the proposed model on the tested dataset, this study has some limitations that should be considered when interpreting its findings and generalizing its application. Primarily, the validation of the model is constrained by its reliance on a standardized dataset, which means its performance under a wider range of real-world conditions has not yet been evaluated. Furthermore, the model's power consumption remains an open question when deployed on hardware with strict memory and processing constraints. Finally, the model's ability to accurately estimate SOC/SOH under unforeseen failure modes or extreme operating conditions outside the training distribution has not been assessed. Addressing these limitations outlines clear pathways for future research, including validation on diverse, multi-source datasets, real-time embedded system implementation, and exploration of the model's transferability across different battery types and operational scenarios.

6 Conclusion and Future Work

Lithium-ion batteries have become an indispensable power source across critical industries and electronic devices due to their reliability and energy efficiency. This research specifically addresses the precise estimation of two fundamental parameters: State of Charge (SOC) and State of Health (SOH) of lithium batteries. In this paper, a novel hybrid OCT-LSTM neural network architecture is proposed. By combining specialized LSTM and Octave networks, the developed framework achieves substantial improvements in both estimation precision and computational performance. A thorough comparative analysis was conducted by implementing and evaluating several benchmark networks, including OCT, LSTM, and CNN-LSTM, to assess their performance relative to the proposed model. Key evaluation metrics included the number of simulation parameters, computational efficiency, and error measures (MSE, RMSE, and MAE). Additionally, dynamic variations in battery SOC and SOH across multiple operational cycles were analyzed.

On the tested NASA dataset, the proposed architecture showed reductions in MSE by 84.53% for SOC estimation and 82.44% for SOH estimation compared to the hybrid CNN-LSTM approach. Furthermore, in comparison with the LSTM network, the improvements are even more pronounced, with MSE reductions reaching 90.57% for SOC and 87.65% for SOH prediction. Notably, the OCT-LSTM network exhibits significant performance enhancements, demonstrating 60.62% and 58.14% lower RMSE rates for SOC and SOH estimation, respectively, when compared to the CNN-LSTM network.

Comparative analysis with the LSTM network reveals further improvements, showing substantial RMSE reductions of 69.28% for SOC and 64.91% for SOH estimation. These performance metrics were obtained using the NASA battery dataset under the specific test conditions described, and the comparative analysis is reliable within the scope of this experimental setup. Moreover, for data-limited scenarios, prediction accuracy can be enhanced through data augmentation, particularly beneficial for short charging cycles. Experimental results demonstrate that the proposed method achieves higher accuracy in SOC and SOH estimation compared to OCT, LSTM, and CNN-LSTM approaches.

Future work can be focused on two key areas to advance this research toward practical application. Foremost, the model's robustness could be tested on a broader range of battery chemistries, including LiCoO2, LiFePO4, and NMC. Moreover, the methodology should be scaled from single-cell to multi-cell and pack-level analysis. This presents challenges such as managing cell-to-cell variations and the complex thermal and electrical interactions within a pack, paving the way for its adoption in next-generation energy storage systems.

Data availability The implementation code for the proposed model and the battery datasets used in this study are publicly available at the following repositories: github.com/seyed-mohammadreza-mousavi/SOH-SOC-estimation for the modeling framework and github.com/Amirhossein-Rahimian-Zarif/NASA_Lithium_Battery_Dataset for the experimental datasets.

Disclosure of Potential Conflicts of Interest

The Authors declare that there is no conflict of interest

Reference

[1] E.O. Ofoegbu, State of charge (SOC) estimation in electric vehicle (EV) battery management systems using ensemble methods and neural networks, J. Energy Storage 114 (2025) 115833. https://doi.org/10.1016/j.est.2025.115833.

[2] G. Chianese, L. Iannucci, O. Veneri, C. Capasso, Real-time estimation of battery SoC through neural networks trained with model-based datasets: Experimental implementation and performance comparison, Appl. Energy 389 (2025) 125783. https://doi.org/10.1016/j.apenergy.2025.125783.

[3] X. Xia, Y. Peng, J. Hu, J. Shen, Z. Chen, State of Health Estimation for Lithium-Ion Batteries Based on Improved Support Vector Regression, 2024 IEEE Transp. Electrif. Conf. Expo, Asia-Pacific, ITEC Asia-Pacific 2024 326 (2024) 472–477. https://doi.org/10.1109/ITECAsia-Pacific63159.2024.10738640.

[4] A. Dannier, G. Brando, M. Ribera, I. Spina, Li-Ion Batteries for Electric Vehicle Applications: An Overview of Accurate State of Charge/State of Health Estimation Methods, Energies 18 (2025) 786. https://doi.org/10.3390/en18040786.

[5] V. Mahadevan, B.P. Vikraman, LSTM based battery management systems and FOPID based cooling system strategy for electric vehicles application, J. Energy Storage 116 (2025) 115937. https://doi.org/10.1016/j.est.2025.115937.

[6] A.R. Zarif, S.A.G. Baygi, Y. Mafinejad, Hybrid Lithium-Ion Portable Renewable Energy Storage System (ESS), in: 2025 6th Int. Conf. Optim. Electr. Energy Consum. OEEC 2025, IEEE, 2025: pp. 1–6. https://doi.org/10.1109/OEEC66525.2025.11100136.

[7] H. Huang, C. Bian, M. Wu, D. An, S. Yang, A novel integrated SOC–SOH estimation framework for whole-life-cycle lithium-ion batteries, Energy 288 (2024) 129801. https://doi.org/10.1016/j.energy.2023.129801.

[8] L. Zhang, S. Wang, S. Wang, B. Zhong, Z. Li, L. Wang, K. Wang, Battery health state prediction based on lightweight neural networks: A review, Ionics (Kiel). 30 (2024) 7781–7807. https://doi.org/10.1007/s11581-024-05857-y.

[9] A.R. Zarif, A. Kazemi, Y. Mafinejad, A Novel Li-Ion Battery Charge Management System for Applying in Renewable Energies Based on Pulse Charge Method, in: 2024 9th Int. Conf. Technol. Energy Manag., IEEE, 2024: pp. 1–6. https://doi.org/10.1109/ICTEM60690.2024.10631901.

[10] P. Dini, D. Paolini, Exploiting Artificial Neural Networks for the State of Charge Estimation in EV/HV Battery Systems: A Review, Batteries 11 (2025) 107. https://doi.org/10.3390/batteries11030107.

[11] P. Li, Z. Zhang, R. Grosu, Z. Deng, J. Hou, Y. Rong, R. Wu, An end-to-end neural network framework for state-of-health estimation and remaining useful life prediction of electric vehicle lithium batteries, Renew. Sustain. Energy Rev. 156 (2022) 111843. https://doi.org/10.1016/j.rser.2021.111843.

[12] S.M. Miraftabzadeh, M. Longo, A. Di Martino, A. Saldarini, R.S. Faranda, Exploring the Synergy of Artificial Intelligence in Energy Storage Systems for Electric Vehicles, Electron. 13 (2024) 1973. https://doi.org/10.3390/electronics13101973.

[13] A.R. Zarif, A. Kazemi, Y. Mafinejad, Reconfigurable Pulse Charge BMS with Pre-Charge Capability for Li-Ion Energy Storage Systems (ESSs), in: 2025 6th Int. Conf. Optim. Electr. Energy Consum. OEEC 2025, IEEE, 2025: pp. 1–6. https://doi.org/10.1109/OEEC66525.2025.11100258.

[14] I. Guedaouria, N. Doghmane, M.F. Harkat, A novel hybrid particle filter optimized by an unscented Kalman filter and genetic algorithm for joint SOC/SOH estimation of li-ion batteries, Ionics (Kiel). 31 (2025) 10719–10746. https://doi.org/10.1007/s11581-025-06663-w.

[15] B.D. Soyoye, I. Bhattacharya, M.V. Anthony Dhason, T. Banik, State of Charge and State of Health Estimation in Electric Vehicles: Challenges, Approaches and Future Directions, Batteries 11 (2025) 32. https://doi.org/10.3390/batteries11010032.

[16] L. Wu, X. Wei, C. Lin, Z. Huang, Y. Fan, C. Liu, S. Fang, Battery SOC estimation with physics-constrained BiLSTM

under different external pressures and temperatures, J. Energy Storage 117 (2025) 116205. https://doi.org/10.1016/j.est.2025.116205.

[17] H. Li, S. Wang, L. Yang, Z. Zhou, Y. Meng, W. Zhang, Z. Shuan, Y. Li, F. Lv, SOH estimation method for lithium-ion battery packs under real-world operating conditions based on a new attenuated model without additional experiments, Energy 330 (2025) 136802. https://doi.org/10.1016/j.energy.2025.136802.

[18] S. Rout, S.K. Samal, D.J. Gelmecha, S. Mishra, Estimation of state of health for lithium-ion batteries using advanced data-driven techniques, Sci. Rep. 15 (2025) 30438. https://doi.org/10.1038/s41598-025-93775-y.

[19] B.P. Saoji, S.D. Wankhade, J.K. Deshmukh, A.M. Gund, J.B. Mandhare, S.M. Satre, M. K. Bhole, Battery Management System in Electric Vehicle for Energy Storage System Using Extended Kalman Filter and Coulomb Counting Methods, Energy Storage 7 (2025) e70139. https://doi.org/10.1002/est2.70139.

[20] M. Dong, X. Li, Z. Yang, Y. Chang, W. Liu, Y. Luo, W. Lei, M. Ren, C. Zhang, State of health (SOH) assessment for LIBs based on characteristic electrochemical impedance, J. Power Sources 603 (2024) 234386. https://doi.org/10.1016/j.jpowsour.2024.234386.

[21] W. Guo, Q. Wang, G. Li, S. Xie, Dual-time scale collaborative estimation of SOC and SOH for lithium-ion batteries based on FOMIRUKF-EKF, Comput. Electr. Eng. 123 (2025) 110048. https://doi.org/10.1016/j.compeleceng.2024.110048.

[22] Y. Liu, A. Lei, C. Yu, T. Huang, Y. Yu, An Improved Collaborative Estimation Method for Determining The SOC and SOH of Lithium-Ion Power Batteries for Electric Vehicles, Energies 17 (2024) 3287. https://doi.org/10.3390/en17133287.

[23] P. Aher, R. Deshmukh, C. Chavan, S. Patil, M. Khare, A. Mandhana, A comprehensive equivalent circuit model of Li-ion batteries for SOC estimation in electric vehicles based on parametric sensitivity analysis, Ionics (Kiel). 31 (2025) 287–303. https://doi.org/10.1007/s11581-024-05950-2.

[24] Y. Zhang, P. Gu, B. Duan, C. Zhang, A hybrid data-driven method optimized by physical rules for online state collaborative estimation of lithium-ion batteries, Energy 301 (2024) 131710. https://doi.org/10.1016/j.energy.2024.131710.

[25] E.I. El-Sayed, S.K. ElSayed, M. Alsharef, Data-Driven Approaches for State-of-Charge Estimation in Battery Electric Vehicles Using Machine and Deep Learning Techniques, Sustain. 16 (2024) 9301. https://doi.org/10.3390/su16219301.

[26] S. Das, S. Samanta, S. Gupta, Online state-of-charge estimation by modified Coulomb counting method based on the estimated parameters of lithium-ion battery, Int. J. Circuit Theory Appl. 52 (2024) 749–768. https://doi.org/10.1002/cta.3806.

[27] C.S. Huang, A Lithium-Ion Batteries Fault Diagnosis Method for Accurate Coulomb Counting State-of-Charge Estimation, J. Electr. Eng. Technol. 19 (2024) 433–442. https://doi.org/10.1007/s42835-023-01533-9.

[28] Y. Fan, Z. Huang, H. Li, M. Bin Kaleem, R. Zhang, W. Liu, State of charge estimation for lithium-ion batteries with enhanced open-circuit voltage model, Meas. J. Int. Meas. Confed. 251 (2025) 117124. https://doi.org/10.1016/j.measurement.2025.117124.

[29] L. Wang, J. Duan, S. Fan, K. Zhao, An estimated value compensation method for state of charge estimation of lithium battery based on open circuit voltage change rate, Energy 313 (2024) 134119. https://doi.org/10.1016/j.energy.2024.134119.

[30] P.R. Dhabe, S.R. Paraskar, S.S. Jadhao, A Comprehensive Analysis of the Open-Circuit Voltage (OCV) Method for the Estimation of State of Charge, Trans. Indian Natl. Acad. Eng. (2025) 1–8. https://doi.org/10.1007/s41403-025-00517-7.

[31] M.A. Pisani Orta, D. García Elvira, H. Valderrama Blaví, Review of State-of-Charge Estimation Methods for Electric Vehicle Applications, World Electr. Veh. J. 16 (2025) 87. https://doi.org/10.3390/wevj16020087.

[32] X. Shu, Y. Li, K. Wei, W. Yang, B. Yang, M. Zhang, Research on the output characteristics and SOC estimation method of lithium-ion batteries over a wide range of operating temperature conditions, Energy 317 (2025) 134726. https://doi.org/10.1016/j.energy.2025.134726.

[33] F. Guo, L.D. Couto, G. Mulder, K. Trad, G. Hu, O. Capron, K. Haghverdi, A systematic review of electrochemical model-based lithium-ion battery state estimation in battery management systems, J. Energy Storage 101 (2024) 113850. https://doi.org/10.1016/j.est.2024.113850.

[34] Y. Xu, X. Ge, R. Guo, W. Shen, Recent advances in model-based fault diagnosis for lithium-ion batteries: A comprehensive review, Renew. Sustain. Energy Rev. 207 (2025) 114922. https://doi.org/10.1016/j.rser.2024.114922.

[35] M.T. Talluri, S. Murugesan, V. Karthikeyan, S. Pragaspathy, The capacity estimation of Li–Ion battery using ML-based hybrid model, Electr. Eng. 107 (2025) 1695–1705. https://doi.org/10.1007/s00202-024-02608-0.

[36] C. Ji, J. Dai, C. Zhai, J. Wang, Y. Tian, W. Sun, A Review on Lithium-Ion Battery Modeling from Mechanism-Based and Data-Driven Perspectives, Processes 12 (2024) 1871. https://doi.org/10.3390/pr12091871.

[37] X. Wu, J. Chen, D. Wang, K. Xu, M. Shao, Y. Wang, Y. Long, Filter-Based Co-Estimation of State-of-Charge and State-of-Health for Lithium-Ion Batteries, IEEE Trans. Ind. Electron. (2025).

[38] P. Takyi-Aninakwa, S. Wang, G. Liu, A.N. Bage, E.D. Bobobee, E. Appiah, Q. Huang, Enhanced extended-input LSTM with an adaptive singular value decomposition UKF for LIB SOC estimation using full-cycle current rate and temperature data, Appl. Energy 363 (2024) 123056. https://doi.org/10.1016/j.apenergy.2024.123056.

[39] L. Breglio, A. Fiordellisi, G. Gasperini, G. Iodice, D. Palermo, M. Tufo, F. Ursumando, A. Mele, A Model-Based Strategy for Active Balancing and SoC and SoH Estimations of an Automotive Battery Management System, Modelling 5 (2024) 911–935. https://doi.org/10.3390/modelling5030048.

[40] L. Kong, Y. Luo, S. Fang, T. Niu, G. Chen, L. Yang, R. Liao, Electrochemical model based SoC-SoH estimation of lithium-ion batteries under shipboard swaying conditions, J. Energy Storage 124 (2025) 116827. https://doi.org/10.1016/j.est.2025.116827.

[41] T. Tang, X. Yang, M. Li, X. Li, H. Huang, C. Guan, J. Huang, Y. Wang, C. Zhou, Deep learning model-based real-time state-of-health estimation of lithium-ion batteries under dynamic operating conditions, Energy 317 (2025) 134697. https://doi.org/10.1016/j.energy.2025.134697.

[42] S. Sun, H. Zhang, J. Ge, L. Che, State-of-health estimation for lithium-ion battery using model-based feature optimization and deep extreme learning machine, J. Energy Storage 72 (2023) 108732. https://doi.org/10.1016/j.est.2023.108732.

[43] Z. Ye, Z.H. Deng, Y.H. Xu, L.F. Lai, R.Q. Zhang, L. Tong, H.G. Zhang, Y.Y. Li, M.H. Gong, G.J. Liu, M.X. Yan, Joint estimation of SOC and SOH for lithium-ion batteries based on FOAMIUHF-UKF model, Sci. Rep. 15 (2025) 1290. https://doi.org/10.1038/s41598-025-24571-x.

[44] Y. Ni, K. Song, L. Pei, X. Li, T. Wang, H. Zhang, C. Zhu, J. Xu, State-of-health estimation and knee point identification of lithium-ion battery based on data-driven and mechanism model, Appl. Energy 385 (2025) 125539. https://doi.org/10.1016/j.apenergy.2025.125539.

[45] H. Thomas, M.H. Weatherspoon, Capacity and State-of-Health Prediction of Lithium-Ion Batteries Using Reduced Equivalent Circuit Models, Batteries 11 (2025) 162. https://doi.org/10.3390/batteries11040162.

[46] L. Jin, F.P. Bereck, J. Granwehr, C. Scheurer, Extending Equivalent Circuit Models for State of Charge and Lifetime Estimation, Electrochem. Sci. Adv. 5 (2025) e202400024. https://doi.org/10.1002/elsa.202400024.

[47] J. Wu, J. Meng, M. Lin, W. Wang, J. Wu, D.I. Stroe, Lithium-ion battery state of health estimation using a hybrid model with electrochemical impedance spectroscopy, Reliab. Eng. Syst. Saf. 252 (2024) 110450. https://doi.org/10.1016/j.ress.2024.110450.

[48] X. Zhao, S. Liu, E. Li, Z. Wang, F. Gu, A.D. Ball, A hybrid intelligent model using the distribution of relaxation time analysis of electrochemical impedance spectroscopy for lithium-ion battery state of health estimation, J. Energy Storage 84 (2024) 110814. https://doi.org/10.1016/j.est.2024.110814.

[49] W. Zhang, R. Ahmed, S. Habibi, State-of-health estimation for lithium-ion batteries based on electrochemical impedance spectroscopy measurements combined with unscented Kalman filter, J. Power Sources 625 (2025) 235450. https://doi.org/10.1016/j.jpowsour.2024.235450.

[50] T. Pham, H. Bui, M. Nguyen, Q. Pham, V. Vu, T. Le, T. Quan, A Comprehensive Review on Data-Driven Methods of Lithium-Ion Batteries State-of-Health Forecasting, Wiley Interdiscip. Rev. Data Min. Knowl. Discov. 15 (2025) e70009.

[51] S.M. Mousavi, A.R. Zarif, J. Hamidzadeh, Lithium Battery SOH Estimation: A Novel Octave and LSTM Hybrid Neural Network Approach, in: 2025 12th Iran. Conf. Renew. Energies Distrib. Gener. ICREDG 2025, IEEE, 2025: pp. 1–6. https://doi.org/10.1109/ICREDG66184.2025.10966104.

[52] J. Gong, B. Xu, F. Chen, G. Zhou, Predictive Modeling for Electric Vehicle Battery State of Health: A Comprehensive Literature Review, Energies 18 (2025) 337. https://doi.org/10.3390/en18020337.

[53] S. Li, Z. Jiang, Z. Zhu, W. Jiang, Y. Ma, X. Sang, S. Yang, A framework of joint SOC and SOH estimation for lithium-ion batteries: Using BiLSTM as a battery model, J. Power Sources 635 (2025) 124624. https://doi.org/10.1016/j.jpowsour.2025.236342.

[54] S. Li, Z. Jiang, Z. Zhu, W. Jiang, Y. Ma, X. Sang, S. Yang, A framework of joint SOC and SOH estimation for lithium-ion batteries: Using BiLSTM as a battery model, J. Power Sources 635 (2025) 236342. https://doi.org/10.1016/j.jpowsour.2025.236342.

[55] M. Ye, G. Lian, W. Li, B. Xia, B. Zhang, Y. Li, Q. Wang, M. Wei, Data-optimization based SOC-SOH estimation for lithium-ion batteries with current bias compensation, Energy 321 (2025) 135490. https://doi.org/10.1016/j.energy.2025.135490.

[56] A. Petrella, M. Marzolla, F. Mercuri, Fast estimation of lithium-ion battery state of health using time series classification, J. Energy Storage 138 (2025) 118747. https://doi.org/10.1016/j.est.2025.118747.

[57] L. Chen, S. Xie, A.M. Lopes, H. Li, X. Bao, C. Zhang, P. Li, A new SOH estimation method for Lithium-ion batteries based on model-data-fusion, Energy 286 (2024) 129597. https://doi.org/10.1016/j.energy.2023.129597.

[58] S.G. Padder, J. Ambulkar, A. Banotra, S. Modem, S. Maheshwari, K. Jayaramulu, C. Kundu, Data-Driven Approaches for Estimation of EV Battery SoC and SoH: A Review, IEEE Access 13 (2025) 35048–35067. https://doi.org/10.1109/ACCESS.2025.3539528.

[59] X. Fang, M. Xu, Y. Fan, SOC-SOH Estimation and Balance Control Based on Event-Triggered Distributed Optimal Kalman Consensus Filter, Energies 17 (2024) 639. https://doi.org/10.3390/en17030639.

[60] T. Yuan, N. Li, H. Sun, S. Tan, A Joint Estimation Method of SOC and SOH for Lithium-ion Battery Considering Cyber-Attacks Based on GA-BP, Comput. Mater. Contin. 80 (2024) 4497–4512. https://doi.org/10.32604/cmc.2024.056061.

[61] C. Li, L. Yang, Q. Li, Q. Zhang, Z. Zhou, Y. Meng, X. Zhao, L. Wang, S. Zhang, Y. Li, F. Lv, SOH estimation method for lithium-ion batteries based on an improved equivalent circuit model via electrochemical impedance spectroscopy, J. Energy Storage 86 (2024) 111167. https://doi.org/10.1016/j.est.2024.111167.

[62] Y. Song, J. Lu, H. Zhang, G. Liu, SOC and SOH Prediction of Lithium-Ion Batteries Based on LSTM–AUKF Joint Algorithm, Energy Sci. Eng. 13 (2025) 240–254. https://doi.org/10.1002/ese3.1992.

[63] T. Çarkıt, M. Alçı, Investigation of Voc and SoH on Li-ion batteries with an electrical equivalent circuit model using optimization algorithms, Electr. Eng. 106 (2024) 1781–1792.

https://doi.org/10.1007/s00202-021-01484-2.

[64] E.H. Jamila, N. Taoufik, A Review of the Estimation of State of Charge (SOC) and State of Health (SOH) of Li-Ion Batteries in Electric Vehicles, World Sustain. Ser. Part F2854 (2024) 519–541. https://doi.org/10.1007/978-3-031-56292-1_42.

[65] G. Chen, H. Zhou, Y. Xu, W. Zhu, L. Chen, Y. Wang, A novel SOC-OCV separation and extraction technology suitable for online joint estimation of SOC and SOH in lithium-ion batteries, Energy 326 (2025) 136246. https://doi.org/10.1016/j.energy.2025.136246.

[66] D. Shen, J. Ding, S. Wang, Parallel neural network combined with adaptive Kalman filter for co-estimation of SOH and SOC of lithium-ion batteries, J. Energy Storage 120 (2025) 116455. https://doi.org/10.1016/j.est.2025.116455.

[67] D. Seo, J. Shin, State-of-Health (SOH)–Based Diagnosis System for Lithium-Ion Batteries Using DNN With Residual Connection and Statistical Feature, Int. J. Energy Res. 2025 (2025) 4046189. https://doi.org/10.1155/er/4046189.

[68] M. Haghighi, M.R. Masoudi, M. Rahimipour Behbahani, Smart Homes Energy Management System Integrated with Renewable Energy Sources and Demand Response Programs, Power, Control. Data Process. Syst. 2 (2025).

[69] M.R. Masoudi, M. Haghighi, M. Rahimipour Behbahani, Optimal Operation of Solar Energy System integrated with Energy Storage Systems, Power, Control. Data Process. Syst. 1 (2024).

[70] M. Monemi Bidgoli, R. Ghani, Optimal Energy Management of Water-Energy Nexus in Multi-Carrier Systems Integrated with Renewable Sources, Power, Control. Data Process. Syst. 1 (2024).

[71] Z. Bao, J. Jiang, C. Zhu, M. Gao, A New Hybrid Neural Network Method for State-of-Health Estimation of Lithium-Ion Battery, Energies 15 (2022) 1–16. https://doi.org/10.3390/en15124399.

[72] L. Zhang, T. Ji, S. Yu, G. Liu, Accurate Prediction Approach of SOH for Lithium-Ion Batteries Based on LSTM Method, Batteries 9 (2023). https://doi.org/10.3390/batteries9030177.

[73] X. Zhang, J. Hou, Z. Wang, Y. Jiang, Joint SOH-SOC estimation model for lithium-ion batteries based on GWO-BP neural network, Energies 16 (2022) 132.

[74] S. Amir, M. Gulzar, M.O. Tarar, I.H. Naqvi, N.A. Zaffar, Dynamic Equivalent Circuit Model to Estimate State-of-Health of Lithium-Ion Batteries, IEEE Access 10 (2022) 18279–18288. https://doi.org/10.1109/ACCESS.2022.3148528.

[75] M. Oza, R. Lamba, R. Kumar, Attention Based Mechanism for State-of-Health Estimation of Li-Ion Batteries, in: 2024 IEEE 4th Int. Conf. Sustain. Energy Futur. Electr. Transp. SEFET 2024, IEEE, 2024: pp. 1–6. https://doi.org/10.1109/SEFET61574.2024.10718141.

[76] S. Bharti, V.K. Saini, A. Kumar Yadav, R. Kumar, A.S. Al-Sumaiti, Optimal Parameter Estimation of CAPN Model for Li-ion Battery, in: 2023 Int. Conf. Comput. Electron. Electr. Eng. Their Appl. IC2E3 2023, IEEE, 2023: pp. 1–6. https://doi.org/10.1109/IC2E357697.2023.10262727.

[77] A. Kumar Yadav, A. Kumar Saini, Dhiraj, Uncertainty aware State-of-Charge estimation for Li-ion Batteries using Deep Learning, in: 2023 2nd IEEE Int. Conf. Meas. Instrumentation, Control Autom. ICMICA 2023, IEEE, 2024: pp. 1–6. https://doi.org/10.1109/ICMICA61068.2024.10732706.

[78] C. Zhang, T. Wang, B. Zhang, L. Qiao, G. Lian, M. Wei, Closed-Loop State of Charge Estimation of Lithium-Ion Batteries Based on Machine Learning and Kalman Filtering, Arab. J. Sci. Eng. (2025) 1–18. https://doi.org/10.1007/s13369-025-10244-4.

[79] R. Sharma, A. Bala, A. Singh, M. Singh, Enhancing Battery Health Monitoring Using a Stacking Approach for Precise and Real-Time State-of-Health Estimation, Arab. J. Sci. Eng. (2025) 1–17. https://doi.org/10.1007/s13369-025-10453-x.

[80] S. Arbaoui, A. Samet, A. Ayadi, T. Mesbahi, R. Boné, Data-driven strategy for state of health prediction and anomaly detection in lithium-ion batteries, Energy AI 17 (2024) 100413. https://doi.org/10.1016/j.egyai.2024.100413.

[81] R. Zheng, B. Yang, Y. Qian, H. Li, D. Gao, L. Jiang, Joint SOH and RUL estimation for lithium-ion batteries via optimal deep belief network with Bayesian algorithm, J. Energy Storage 114 (2025) 115891. https://doi.org/10.1016/j.est.2025.115891.

[82] C.L. Sravanthi, J.N. Chandra Sekhar, N.C. Alluraiah, C. Dhanamjayulu, H. Kumar Pujari, B. Khan, An Overview of Remaining Useful Life Prediction of Battery Using Deep Learning and Ensemble Learning Algorithms on Data-Dependent Models, Int. Trans. Electr. Energy Syst. 2025 (2025) 2242749. https://doi.org/10.1155/etep/2242749.

[83] J. Chen, P. Li, L. Wu, Joint prediction of SOH and RUL of lithium-ion batteries using single-cycle charging data, Energy 336 (2025) 138351. https://doi.org/10.1016/j.energy.2025.138351.

[84] G. Patrizi, L. Martiri, A. Pievatolo, A. Magrini, G. Meccariello, L. Cristaldi, N.D. Nikiforova, A Review of Degradation Models and Remaining Useful Life Prediction for Testing Design and Predictive Maintenance of Lithium-Ion Batteries, Sensors 24 (2024) 3382. https://doi.org/10.3390/s24113382.

[85] H. Cao, X. Lian, L. Chen, Z. Duan, A computationally efficient and lightweight model for high-accuracy OCT image classification, World Wide Web 28 (2025) 35. https://doi.org/10.1007/s11280-025-01348-w.

[86] Z. Guo, Z. Zhao, Hybrid attention structure preserving network for reconstruction of under-sampled OCT images, Sci. Rep. 15 (2025) 7405. https://doi.org/10.1038/s41598-024-82812-x.

[87] J. Hu, R. Liu, Z. Chen, D. Wang, Y. Zhang, B. Xie, Octave convolution-based vehicle detection using frame-difference as network input, Vis. Comput. 39 (2023) 1503–1515. https://doi.org/10.1007/s00371-022-02425-1.

[88] J.A. Diaz-Madrid, G. Domenech-Asensi, R. Ruiz-Merino, J.F. Zapata-Perez, A real-time and energy-efficient SRAM with mixed-signal in-memory computing near CMOS sensors, J. Real-Time Image Process. 21 (2024) 143. https://doi.org/10.1007/s11554-024-01520-x.

[89] B. Saha, K. Goebel, Uncertainty management for diagnostics

and prognostics of batteries using Bayesian techniques, in: 2008 IEEE Aerosp. Conf., IEEE, 2008: pp. 1–8.

[90] B. Bole, C. Kulkarni, M. Daigle, Randomized battery usage data set, NASA AMES Progn. Data Repos. 70 (2014).

[91] H. Sun, J. Sun, K. Zhao, L. Wang, K. Wang, Data-Driven ICA-Bi-LSTM-Combined Lithium Battery SOH Estimation, Math. Probl. Eng. 2022 (2022) 1–8. https://doi.org/10.1155/2022/9645892.

Nomenclature

Abbreviations		PCoE	Prognostics Center of Excellence
EV	electric vehicles	mAh	milliampere-hour
LSTM	long short-term memory	mA	milliampere
OctConv	octave convolution	Ah	ampere-hour
MSE	mean squared error	V	voltage
RMSE	root mean squared error	CC	constant current
MAE	mean absolute error	CV	constant voltage
ReLU	rectified linear unit	EOL	end of life
CNN	convolutional neural network	PV	photovoltaics
OCT	octave convolution	SCA	sine cosine algorithm
CNN-LSTM	convolutional neural network-long short-term memory	DE	differential evolution
OCT-LSTM	octave convolution- long short-term memory	HHO	Harris Hawks optimization
SOC	state of charge	CPDE	cycle-preserved data expansion
SOH	state of health		
LIB	lithium-ion battery	**Notations**	
ESS	energy storage system	X	input tensor
CCM	Coulomb counting method	B	batch size
OCV	open-circuit voltage	T	time dimension
ML	machine learning	F	feature dimension
RBF-ARX	radial basis function auto-regressive models with exogenous inputs	C	channel dimension
BiLSTM	bidirectional LSTM	R	real numbers
PSO	particle swarm optimization	X_H	high frequency
EKF	extended Kalman filter	X_L	low frequency
ECM	equivalent circuit model	H→H	High-to-high
FPSO-CL	fractional-order dynamics and crisscross learning	H→L	High-to-low
KCF	Kalman consensus filter	L→H	Low-to-high
BMS	battery management systems	L→L	Low-to-low
ETM	event-triggering mechanism	Y_H^{HH}	high-to-high convolution output
EIS	electrochemical impedance spectroscopy	W_{HH}	convolutional weight matrix for the high-to-high frequency pathway
BES	battery energy storage	∗	convolution operator
ABC	artificial bee colony	Y_L^{HL}	high-to-low convolution output
DA	dragonfly algorithm	W_{HL}	convolutional weight matrix for the high-to-low frequency pathway
GA	genetic algorithm	↓	down-sampling operation
PNN	parallel neural network	Y_H^{LH}	low-to-high convolution output
BPNN	back propagation neural network	W_{LH}	convolutional weight matrix for the low-to-high frequency pathway
ENN	Elman neural network	↑	up-sampling operation
AKF	adaptive Kalman filter	Y_L^{LL}	low-to-low convolution output
R-DNN	residual-deep neural network	W_{LL}	convolutional weight matrix for the low-to-low frequency pathway
CNN-BiGRU	convolutional neural network-bidirectional gated recurrent unit	Y_H	high-frequency output
RNN	recurrent neural network	Y_L	low-frequency output
GWO-BP	grey wolf optimization-back propagation	Y	integration of both high-frequency and low-frequency
GWO	grey wolf optimization	X_i^k	normalized parameters
LR	linear regression	n	number of samples per cycle
Ah	ampere-hour	x	collection of all charge cycles
2-RC	second-order resistor and capacitor	Q_r	remaining battery charge or remaining charge capacity
N-RC	n-order resistor and capacitor	$Q_{nominal}$	nominal capacity
1-RC	first-order resistor and capacitor	C_r	battery capacity
RUL	remaining useful life	C_c	capacity for each discharge cycle
XGBoost	extreme gradient boosting	y_i	modeled capacity
RF	random forest	$\hat{y}_i$	actual capacity